Environ. Sci. Technol. **2010,** *44,* 1638–1643

Photo-Oxidation of Low-Volatility Organics Found in Motor Vehicle Emissions: Production and Chemical Evolution of Organic Aerosol Mass

MARISSA A. MIRACOLO,[†] ALBERT A. PRESTO,[†] ANDREW T. LAMBE,[†] CHRISTOPHER J. HENNIGAN,[†] NEIL M. DONAHUE,[†] JESSE H. KROLL,[‡] DOUGLAS R. WORSNOP,[§] AND ALLEN L. ROBINSON*,[†]

Departments of Mechanical Engineering and Chemical Engineering and Center for Atmospheric Particle Studies, Carnegie Mellon University, Pittsburgh, Pennsylvania 15213, Massachusetts Institute of Technology, Cambridge, Massachusetts 02139, and Aerodyne Research, Inc., Billerica, MA 01821

Received August 31, 2009. Revised manuscript received December 17, 2009. Accepted January 7, 2010.

Recent research has proposed that low-volatility organic vapors are an important class of secondary organic aerosol (SOA) precursors. Mixtures of low-volatility organics were photo-oxidized in a smog chamber under low- and high-NO_x conditions. Separate experiments addressed emission surrogates (diesel fuel and motor oil) and single components (*n*-pentacosane). Both diesel fuel and motor oil are major components of exhaust from diesel engines. Diesel fuel is a complex mixture of intermediate volatility organic compounds (IVOCs), whereas motor oil is a complex mixture of semivolatile organic compounds (SVOCs). IVOCs exist exclusively in the vapor phase, while SVOCs exist in both the aerosol and vapor phase. Oxidation of SVOC vapors (motor oil and *n*-pentacosane) creates substantial SOA, but this SOA is largely offset by evaporation of primary organic aerosol (POA). The net effect is a cycling or pumping of SVOCs between the gas and particle phases, which creates more oxygenated organic aerosol (OA) but little new OA mass. Since gas-phase reactions are much faster than heterogeneous ones, the processing of SVOC vapors likely contributes to the production of highly oxidized OA. The interplay between gas−particle partitioning and chemistry also blurs traditional definitions of POA and SOA. Photo-oxidation of diesel fuel (IVOCs) rapidly creates substantial new OA mass, similar to published aging experiments with dilute diesel exhaust. However, aerosol mass spectrometer (AMS) data indicated that the SOA formed from emission surrogates is less oxidized than either the oxygenated organic aerosol (OOA) measured in the atmosphere or SOA formed from the photo-oxidation of dilute diesel exhaust. Therefore, photo-oxidation of IVOCs helps explain the substantial SOA mass produced from aging diesel exhaust, but some component is missing from these emission surrogate experiments that leads to the rapid production of highly oxygenated SOA.

* Corresponding author e-mail: alr@andrew.cmu.edu.
[†] Carnegie Mellon University.
[‡] Massachusetts Institute of Technology.
[§] Aerodyne Research, Inc.

Introduction

Organic aerosol (OA) comprises particles directly emitted from sources (primary organic aerosol or POA) and aerosol formed from low-volatility products of gas-phase reactions (secondary organic aerosol or SOA). State-of-the-art atmospheric chemistry models cannot reproduce the high levels of rapid production of SOA observed in urban environments and in smog chamber experiments with dilute emissions (*1*−*3*). Recent research has proposed that low-volatility organic vapors may be important SOA precursors (*2, 4, 5*). Emissions of these vapors are substantial (*5*−*7*), but they are poorly represented in air-quality models (*2, 5*).

This research investigated SOA formation from two classes of low-volatility organic vapors: intermediate volatility organic compounds (IVOCs) and semivolatile organic compounds (SVOCs). A compound is classified as an IVOC or SVOC based on its effective saturation concentration (C^*). IVOCs include all compounds with C^* values between 10^6 and 10^3 $\mu g\ m^{-3}$, which, for example, correspond to C_{13}−C_{20} *n*-alkanes (*8, 9*). SVOCs include all compounds with C^* values between 10^3 and 10^{-1} $\mu g\ m^{-3}$, which corresponds to C_{21}−C_{32} *n*-alkanes (*8, 9*). IVOCs exist as vapors in the atmosphere, whereas SVOCs partition between the particle and vapor phase. Both IVOCs and SVOCs are much less volatile than the single-ring aromatics and monoterpenes that dominate SOA formation in current atmospheric chemistry models.

We are not aware of any data on SOA production from SVOCs, but recent experiments have begun to investigate SOA production from IVOCs. Lim and Ziemann (*10*) show SOA yields from alkanes depend on both precursor volatility and molecular structure. Chan et al. (*11*) report high SOA yields from naphthalenes. Presto et al. (*12*) showed that oxidation of large *n*-alkanes can create highly oxygenated organic aerosol. Although *n*-alkanes and naphthalenes appear to be important SOA precursors, they only contribute a small fraction of the IVOC and SVOC mass emitted by combustion systems. Since the vast majority of the IVOC and SVOC mass has not been identified on a molecular basis (*7*), it is difficult to quantify the SOA formation of diesel exhaust or other emissions using data from traditional single precursor experiments.

This paper describes experiments that photo-oxidized motor vehicle emission surrogates and individual *n*-alkanes. We report changes in aerosol mass and chemical composition. By conducting experiments with increasingly complex mixtures of precursors we hope to better understand the relationship between traditional single precursor experiments and the atmosphere.

Experimental Methods

Experiments were performed in the Carnegie Mellon University smog chamber, a 10 m^3 Teflon bag suspended in a temperature-controlled room. Before each experiment, the chamber was cleaned by heating, flushing with HEPA and activated carbon filtered air, and irradiation with UV lights for a minimum of 12 h.

Separate experiments were conducted with diesel fuel, motor oil, a 3:1 mixture of diesel fuel and motor oil, and *n*-pentacosane. Unburned diesel fuel and motor oil are major components of emissions from diesel engines; a 3:1 diesel-fuel/motor-oil mixture reproduces the *n*-alkane distribution in the Schauer et al. (*7*) diesel emission profile.

Motor oil and diesel fuel are complex mixtures of hydrocarbons. Chromatograms of the motor oil and motor-oil-plus-diesel-fuel mixture are shown in Figure S1 (see

10.1021/es902635c

Published on Web 02/01/2010

Supporting Information). Diesel fuel is a mixture of IVOCs, with carbon numbers ranging from C_8 to C_{25} and a peak around C_{14} (*13, 14*). The diesel fuel used in these experiments contained 26% aromatics and 74% alkanes. Motor oil is a complex mixture of SVOCs with carbon numbers between C_{20} and C_{36}. The dominant feature of the motor oil chromatogram is the UCM hump; motor oil aerosols evaporate upon isothermal dilution and gentle heating (*15*).

The emission surrogates were flash vaporized into the chamber. Photo-oxidation was conducted under high- and low-NO_x conditions using two different hydroxyl radical (OH) sources. For the high-NO_x experiments, HONO was photolyzed to produce OH; for the low-NO_x experiments HOOH was photolyzed. Photo-oxidation was initiated by turning on the chamber UV lights (General Electric model 10526), which yield an NO_2 photolysis rate of 0.2 min^{-1} (*16*).

OH concentrations were inferred from the measured decay of *n*-pentane and published kinetic data (*17*). The HONO source generated $\sim(1-4) \times 10^7$ molecules cm^{-3} of OH for the first hour after the UV lights were turned on and $\sim 1 \times 10^6$ molecules cm^{-3} for the rest of the experiment. The fall off in OH is due to the majority of the HONO being photolyzed in the first hour of the experiment. Irradiation of the HOOH source created a relatively constant [OH] concentration of $\sim(1-3) \times 10^6$ molecules cm^{-3} throughout an experiment.

The evolution of the gas- and particle-phase material inside the chamber was characterized using a suite of instruments, including a scanning mobility particle sizer (SMPS) and either an Aerodyne quadrupole aerosol mass spectrometer (Q-AMS) or an Aerodyne high-resolution time-of-flight aerosol mass spectrometer (HR-AMS). Details on the OH sources and instrumentation are provided in the Supporting Information.

We use the approach of Weikamp et al. (*4*) to correct the data for loss of particles and semivolatile vapors to the smog chamber walls. The biggest uncertainty is the treatment of the losses of condensable vapors. We consider two limiting cases: condensable vapors partition only to suspended particles and condensable vapors remain in equilibrium. Details on wall loss correction are provided in the Supporting Information.

Results

Figure 1 shows results from high-NO_x photo-oxidation experiments of the motor-oil-plus-diesel-fuel mixture, motor oil, and *n*-pentacosane. Initial POA concentrations ranged from 5 to 86 $\mu g\ m^{-3}$. Each plot shows the evolution of the wall loss corrected mass concentration measured with the SMPS (assuming unit density and spherical particles). The wall loss corrected data plotted in Figure 1 assume that condensable products only partition to suspended particles. Since some condensable vapors are lost to the walls, the results in Figure 1 provide a lower bound estimate of the SOA production.

Figure 1a indicates that high-NO_x photo-oxidation of the motor-oil-plus-diesel-fuel mixture creates substantial new aerosol mass, doubling the suspended OA concentrations after only 30 min of exposure to $\sim 3 \times 10^7$ molecules cm^{-3} of OH. The production of new OA mass then slows as the OH levels in the chamber drop. A very different behavior was observed in the experiments with pure motor oil. Figure 1b indicates that high-NO_x photo-oxidation of motor oil created relatively little new OA mass, increasing wall-loss corrected OA concentrations by about 13% in the first hour of oxidation. Therefore, the addition of diesel fuel into the motor oil significantly increased the production of new OA mass. This hypothesis was confirmed by photo-oxidizing pure diesel fuel which created a burst in OA formation similar to that observed in the motor-oil-plus-diesel-fuel experiments.

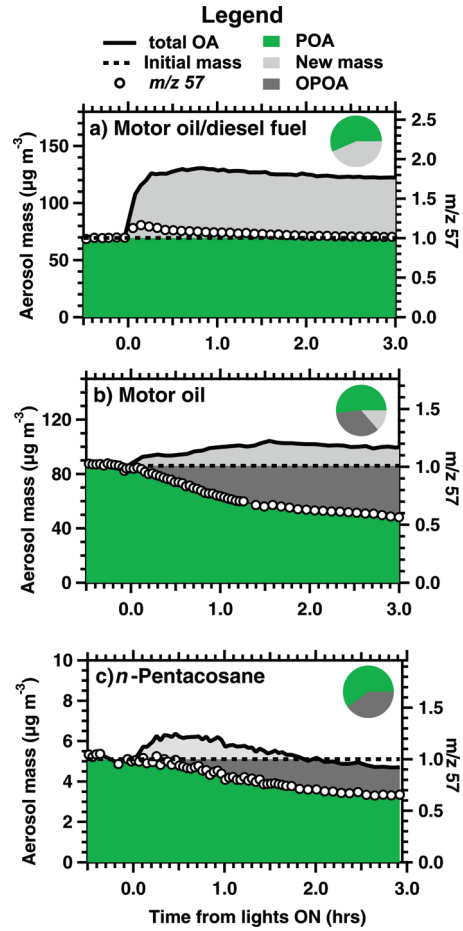

FIGURE 1. Wall-loss corrected OA mass concentrations for (a) motor oil, (b) motor-oil-plus-diesel-fuel mixture, and (c) *n*-pentacosane experiments. The normalized, wall-loss-corrected decay of the absolute AMS *m/z* 57 signal is plotted on the right axis. This trace has been normalized by the initial ($t = 0$) *m/z* 57 signal. The shaded areas show the contribution of primary organic aerosol (POA, green area), oxidized POA (dark gray area), and new OA mass (light gray area) to the total mass. These different classes of material are defined in the text. The pie charts show the relative composition at the end of the experiment. Horizontal dashed line indicates the wall-loss corrected initial mass.

To quantitatively compare the OA production in different experiments, Figure 2 plots OA mass enhancement for several experiments as a function of integrated OH exposure. One cannot define a traditional SOA yield in these experiments because that requires measuring the decay of every species in the emission surrogates. The mass enhancement is the ratio of the wall-loss corrected OA concentration to the wall-loss corrected POA concentration. Figure 2 indicates that high-NO_x photo-oxidation of motor oil produces about an order of magnitude more new OA mass than motor oil per unit OH exposure.

To illustrate the uncertainty associated with wall-loss correction, Figure 2 also plots both the upper and lower bound estimates for the change in OA mass. The lower bound estimates are also shown in Figure 1; they assume condensable vapors only partition to the suspended particles. The upper bound estimates quantify the loss of condensable vapors to the walls by assuming the particle losses to the walls remain in equilibrium with the vapors (*4*). For the high-NO_x experiments there is little difference between these two estimates; therefore, our conclusions regarding the OA formation potential of diesel fuel and motor oil are not sensitive to uncertainties in the wall loss correction.

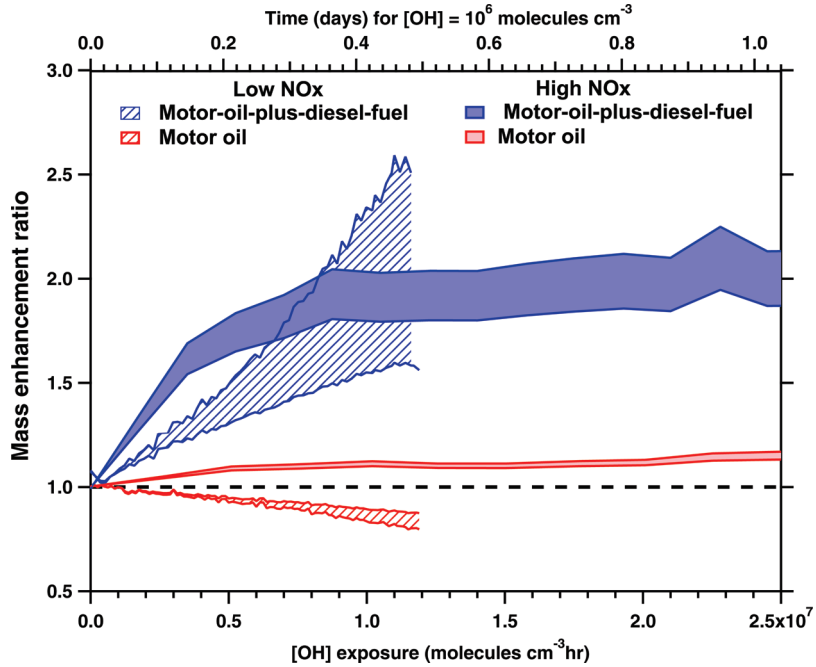

FIGURE 2. Organic aerosol mass enhancement ratio for motor oil and motor-oil-plus-diesel-fuel experiments conducted under low and high-NO_x conditions as a function of OH exposure. Mass enhancement is the ratio between the wall-loss corrected aerosol concentration and the estimated POA concentration. The shaded areas indicate uncertainty in the wall-loss corrections, as discussed in the text, the upper estimates account for loss of condensable vapors to the chamber walls; the lower estimates assume only particles are lost to the walls.

In our discussion of Figures 1 and 2, we have been careful to describe the results in terms of changes of OA mass and not SOA production. One might be tempted to equate these two quantities, but that requires that the POA be nonvolatile and nonreactive (*2*). However, this is not the case and the AMS data reveal substantial processing of the POA in the pure motor oil experiments.

The AMS signal at m/z 57 ($C_4H_9^+$) is often used as a tracer for POA (*18*). m/z 57 is an imperfect tracer because oxidized fragments associated with SOA can also contribute to the signal (*19*). Measurements with the HR-AMS indicate that by the end of an experiment about 15−20% of the signal at m/z 57 was due to the $C_3H_5O^+$ fragment. In addition, SOA formed from *n*-alkanes also produces $C_4H_9^+$ fragments (*12*). Therefore, the AMS m/z 57 signal provides a conservative, upper bound estimate for the POA concentrations in the chamber, overestimating it by at least 15−20% at the end of the experiment. One can directly compare the wall-loss-corrected SMPS and AMS data in these experiments because the SMPS total particle volume calculated assuming spherical particles and the AMS total organic mass were strongly correlated (linear correlation $R^2 = 0.94$ or higher) indicating that the particle density and collection efficiency did not change with photo-oxidation.

Figure 1 also plots time series of the normalized, wall-loss-corrected m/z 57 signal. For the pure motor-oil experiments, the AMS m/z 57 signal shows that the POA concentrations decays much faster than the wall loss rate (Figure 1b). This was not observed in the motor-oil-plus-diesel-fuel experiments (Figure 1a). In those experiments, the AMS signal at m/z 57 initially increased, indicating that some of the compounds in the SOA contribute to the signal at m/z 57. The m/z 57 signal then decayed modestly faster than the measured wall-loss rate for the rest of the experiment.

There are two possible explanations for the unexpectedly rapid decay of the AMS POA tracer fragments in the pure motor oil experiments: heterogeneous oxidation or evaporation of the POA. To evaluate the first hypothesis, we compared the OH collision rate to the wall-loss corrected decay rate of the AMS POA tracer fragments to determine whether or not the measured decay could be explained by heterogeneous OH oxidation. This was done by calculating an effective uptake coefficient (*20*).

$$\gamma_{\text{eff}} = \frac{2}{3}\frac{k_{\text{OH}} D \rho N_{\text{a}}}{\bar{c} M f_{\text{diff}}} \qquad (1)$$

where D is the mean surface area weighted particle diameter, ρ is the density of the particle (1 g cm^{-3}), M is the mean molecular mass (394 g mol^{-1} which corresponds to a C_{28} *n*-alkane), N_a is Avogadro's number, $\bar{c}$ is the mean molecular speed of the oxidant, and f_{diff} is the Fuchs−Sutugin correction factor (*21*). The oxidation rate (k_{OH}) was estimated by fitting a linear regression to the wall-loss corrected decay of alkyl fragments such as m/z 57 measured with the AMS versus OH exposure, as shown in Figure 3. Figure 3 plots the wall-loss corrected decay of m/z 57, 71, and 85 from a high-NO_x motor oil photo-oxidation experiment. The dashed line shows the calculated decay corresponding to $\gamma_{\text{eff}} = 1$.

Effective uptake coefficients with values greater than one indicate that the decay rate of the AMS tracer fragments is faster than the OH collision rate. The effective uptake coefficients for the alkyl fragments range from $\gamma_{\text{eff}} = 5.0 \pm 1.0$ to 6.2 ± 1.8. Since SOA also contributes to the AMS signal at these mass fragments, these are lower-bound estimates for the effective uptake coefficients.

To attribute the surprisingly large effective uptake coefficients to heterogeneous chemistry requires that each OH collision initiate multiple secondary reactions. Previous studies have reported effective heterogeneous uptake coefficients of two, indicating one secondary reaction for each OH collision (*22*). Therefore, explaining the measured decay of the AMS tracer fragments requires almost three times more secondary chemistry than has been previously reported. This seems highly unlikely.

The second explanation for the rapid decay of the AMS POA tracer fragments is evaporation. Gas-phase oxidation

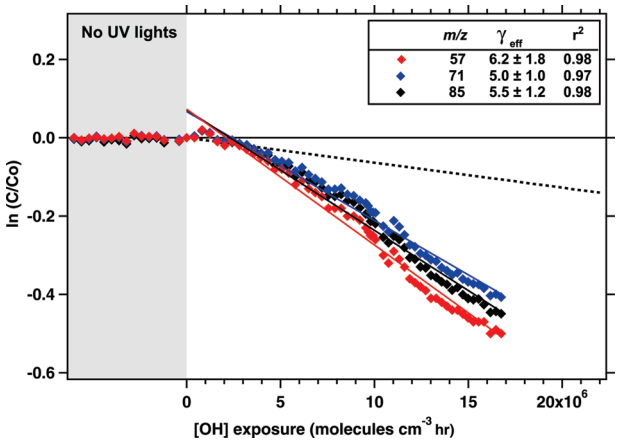

FIGURE 3. Wall-loss-corrected AMS tracer fragment *m/z* 57, 71, and 85 signals from motor oil experiment. C/C_0 is the ratio of the wall-loss-corrected signal to the initial signal (before oxidation). The analysis is based on the absolute (not relative) AMS signal and therefore is not affected by dilution associated with the formation of new aerosol mass. Dashed line indicates decay corresponding to an effective uptake coefficient equal to 1. Solid horizontal line indicates no change in tracer fragments. AMS signal for these fragments falls at the same rate as the wall-loss rate before UV lights are turned on.

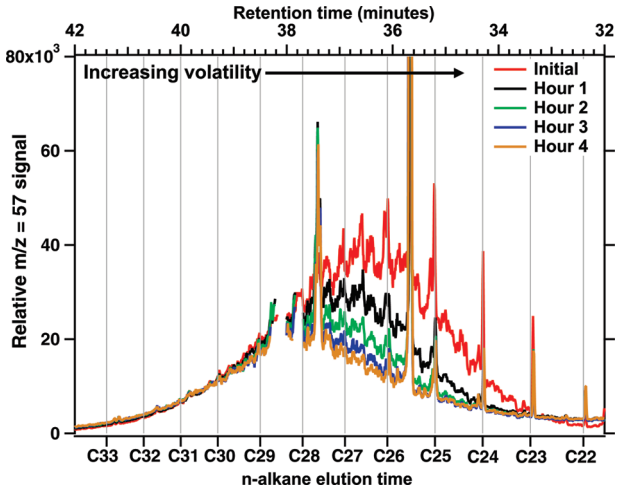

FIGURE 4. TAG chromatograms of *m/z* 57 measured in a high-NO_x motor-oil-plus-diesel-fuel photo-oxidation experiment. As described in the text, the chromatograms are normalized by the TAG signal for a C_{30} *n*-alkane to isolate the relative changes in POA mass as a function of volatility. For the conditions of these experiments, a C_{25} *n*-alkane is partitioned about 50:50 between the gas and particle phases. Vertical lines indicate elution times of *n*-alkanes between C_{22} and C_{33}.

reduces SVOC vapor concentrations, which, in turn, forces some of the particle-phase SVOCs to evaporate to maintain thermodynamic phase equilibrium. This creates competition between formation of new aerosol mass via oxidation of SVOC vapors and evaporation of particle-phase SVOCs. The net effect is that SVOCs cycle through the gas phase, creating a more oxidized aerosol without significant mass increases.

Although a strong thermodynamic argument can be made for the evaporation hypothesis, it is also supported by a variety of experimental data. For example, Figure 4 shows a series of TAG chromatograms of m/z 57 measured during a high-NO_x motor-oil-plus-diesel-fuel mixture oxidation experiment. m/z 57 is a prominent fragment formed from electron impact ionization of hydrocarbons and the GC column used in TAG separates hydrocarbons and other low-polarity organics found in POA based on boiling point or volatility (*23*). The most prominent feature of the TAG chromatograms is the large hump commonly referred to as UCM that elutes between 32 and 42 min, which spans the volatility range of SVOCs. UCM is the dominant component of POA (*7*). To isolate the effects of photo-oxidation of the UCM/POA signal, each TAG chromatogram has been normalized by the C_{30} signal of the unoxidized POA chromatogram. Therefore, Figure 4 reveals relative changes in the UCM/POA as a function of volatility.

Figure 4 indicates there is no change in the normalized concentration of the heavier fraction of the UCM signal eluting after roughly a C_{28} alkane. However, photo-oxidation reduced the concentration of the semivolatile fraction of the UCM that elutes between approximately *n*-C_{23} and *n*-C_{28}. This relative change in the UCM highlights the faster gas-phase oxidation that results in preferential removal of the semivolatile fraction of the UCM. We attribute this decrease to evaporation of particle-phase SVOCs present in motor oil driven by gas-phase oxidation of those vapors.

The evaporation hypothesis was further explored by conducting experiments with *n*-pentacosane, an SVOC. Figure 1c shows results from a typical high-NO_x photo-oxidation experiment. Immediately after the UV lights are turned on, the suspended aerosol mass concentration increases indicating production of new OA mass. However, after about 30 min of oxidation, the aerosol mass starts decreasing at a rate faster than the wall-loss rate. After 2 hours of photo-oxidation, the suspended aerosol mass matches the estimated POA mass, indicating there was no net production of new aerosol mass. Although there was no net production over the course of the experiment, the AMS data indicate that the OA became more oxidized.

Figure 1c also shows that the AMS m/z 57 signal decays faster than the wall-loss of *n*-pentacosane. The effective uptake coefficient calculated from the wall-loss corrected decay of m/z 57 is $\gamma_{eff} = 3.9 \pm 0.9$. Therefore, the loss of m/z 57 signal cannot be explained by heterogeneous chemistry.

The production of some new OA mass in the first half an hour of the *n*-pentacosane experiments indicates that the evaporation rate is relatively slow. When OH levels are high, the oxidation rate exceeds the *n*-pentacosane evaporation rate resulting in the net production of new mass. However, later in the experiment (when OH levels are an order of magnitude lower) evaporation catches up and even though *n*-pentacosane vapors continue to be oxidized there is no production of new aerosol mass. The relatively slow evaporation observed here is similar to that measured in dilution experiments with α-pinene SOA (*24*) and motor oil (*15*).

The only experiments in which we did not observe substantial loss of wall-loss corrected POA were those with diesel fuel (Figure 1a). However, the m/z 57 signal from the SOA mass may mask the loss of POA. In addition, the SOA and POA in these experiments do not form a single organic phase (*25*), potentially slowing the evaporation of the POA.

Previous research has shown that SOA yields depend on the VOC/NO_x ratio (*12, 16*). Figure 2 compares mass enhancement for the motor oil and motor-oil-plus-diesel-fuel plotted as a function of OH exposure to allow for quantitative comparisons between the low- and high-NO_x experiments. Figure 2 suggests there may be some differences in OA production for low- and high-NO_x cases. For example, there is modest (~10%) loss of wall loss corrected OA mass in the low-NO_x oxidation of motor oil versus modest production (~10%) from high-NO_x experiments. This difference was consistently seen across repeated experiments. For the motor-oil-plus-fuel experiments, there is substantial uncertainty in the wall loss corrected mass in the low-NO_x experiments, which makes it difficult to draw any conclusions regarding the effects of NO_x. This simply reflects the fact that

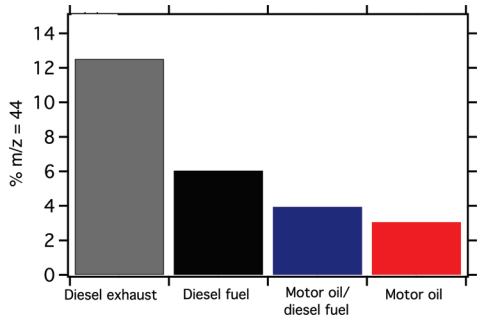

FIGURE 5. Average contribution of *m/z* 44 in the AMS SOA spectra formed from photo-oxidation of each emission surrogate and diesel exhaust. These values are averages of data from multiple experiments (low- and high-NO_x) at similar levels of OH exposure. Diesel exhaust data are from Sage et al. (*18*).

the uncertainty in the wall loss correction increases as an experiment progresses (*4*).

Secondary Organic Aerosol Composition. The AMS signal at m/z 44 is a measure of the extent of oxidation of the SOA (*26*). Figure 5 compiles data on the average contribution of m/z 44 to the SOA mass. For experiments with POA, the mass spectra of the SOA was estimated using the method of Sage et al. (*18*).

Figure 5 compares the contribution of m/z 44 to the SOA formed from the different emission surrogates exposed to similar levels of OH (time series of these data are shown in the Supporting Information). As expected, the SOA is more oxidized compared to the POA. For example, m/z 44 contributes 0.6% of the organics in unoxidized motor oil versus 3% in the SOA formed from photo-oxidation of motor oil. However, the SOA formed from all of these surrogates is significantly less oxidized than SOA formed from photo-oxidation of actual exhaust. The most oxidized SOA (m/z 44 of 6%) was formed from diesel fuel, but this is a factor of 2 smaller than that formed from photo-oxidation of actual diesel exhaust.

Of the three emission surrogates, photo-oxidation of diesel fuel created the most oxygenated SOA, followed by the motor-oil-plus-diesel-fuel mixture, and finally pure motor oil. Presto et al. (*12*) hypothesized that these differences are due in part to differences in gas−particle partitioning. First-generation oxidation products of SVOCs partition into the particle phase and therefore do not undergo multiple generations of oxidation. However, some of the first generations products of IVOCs (diesel fuel) are vapors that can undergo multiple generations of oxidation. Another factor is that less volatile vapors in the motor oil experiments require less oxidation (fewer added oxygen molecules) to shift them into the condensed phase than the smaller, more volatile molecules found in diesel fuel. The level of oxidation of the SOA also appears to depend weakly on organic aerosol concentration (Figure S2 Supporting Information).

Discussion

Photo-oxidation of SVOCs and IVOCs highlights how partitioning and chemistry interact to influence the production and chemical evolution of OA. The coupling of partitioning and chemistry also blurs traditional definition of SOA and POA. SOA has traditionally been defined as OA formed from the reaction products of gas-phase precursors (*27*), which implies that SOA formation creates new OA mass. POA has traditionally been defined as nonvolatile, inert OA directly emitted by sources (*27*). However, the motor oil and *n*-pentacosane experiments illustrate that these definitions break down in systems with substantial SVOCs.

To discuss these issues, Figure 1 separates the total OA into three classes of material: POA, oxidized POA (OPOA), and new OA. POA is the unreacted primary emissions, defined by the AMS POA tracer fragments (m/z 57, 71, 85, etc.). OPOA is OA formed from the oxidation of SVOC vapors that is offset by the evaporation of semivolatile POA. Finally, "new OA" is the difference between wall loss corrected concentration and the initial concentration. The pie charts shown in Figure 1 quantify the contribution of each of these classes to the total OA at the end of each experiment.

New OA is clearly SOA. OPOA could also be classified SOA because it is formed from gas-phase reactions, but it is different from traditional SOA in that it does not result in a net increase OA concentrations. Figure 1 shows that significant amounts of OPOA were formed in the *n*-pentacosane and motor oil experiments. If one defines SOA as OA formed from gas-phase reactions, then SOA is OPOA plus new OA mass. Based on this definition, similar amounts of SOA were formed in every experiment, even though little or no new OA mass was formed in the motor-oil and *n*-pentacosane experiments, respectively. Therefore, the traditional definitions of POA and SOA do not account for the significant conversion of semivolatile POA into OPOA and one must be careful when defining SOA yields for systems with substantial SVOCs.

Experiments with IVOCs resulted in substantial SOA formation and production of new OA mass. IVOCs, like traditional SOA precursors such as single-ring aromatics, exist exclusively in the vapor phase, therefore oxidation does not lead to evaporation. Although SOA formation from IVOCs has not traditionally been accounted for in chemical transport models, combustion sources emit substantial amounts of IVOCs and significant amounts of IVOC have also been observed in the atmosphere (*5*). Therefore, IVOCs are likely an important source of SOA mass in the atmosphere.

Although the motor-oil-plus-diesel-fuel experiments produced substantial OA mass similar to that observed in experiments with dilute diesel exhaust, the level of oxidation of the SOA formed from the emission surrogate is significantly less than SOA formed from dilute diesel exhaust (*26*) and ambient oxygenated organic aerosol (OOA) factors (*28*). This is not surprising since these emission surrogates are complex mixtures of organic material, a significant fraction of which consists of long chain hydrocarbons. Each generation of oxidation can add up to three oxygen atoms (*29*); therefore, without breaking the carbon backbone, multiple generations of oxidation are required to create SOA with high oxygen-to-carbon ratios. Therefore, there is some component missing in the emission surrogate experiments necessary to explain the extent of oxidation measured in the experiments with actual diesel exhaust. This component is presumably associated with partially burned fuel or oil. Recent phase partitioning experiments by Asa-Awuku et al. (*25*) also reveal that motor-oil-plus-fuel mixtures are imperfect surrogates for actual emissions.

The cycling of SVOCs observed here may help explain the OA transformations observed in recent aircraft studies of evolving plumes (*19, 30*). For example, Capes et al. (*30*) reported that aging of biomass burning plumes in Africa created more oxidized OA with little change in aerosol mass. This is consistent with the cycling observed in the SVOC experiments. Since gas-phase reactions are much faster than heterogeneous ones, the processing of SVOC in the gas-phase likely contributes to the production of highly oxidized organic aerosol. This behavior underscores that OA are a highly dynamic system with material evaporating, recondensing, and reacting in both the gas and particle phases.

Acknowledgments

This work was supported by the EPA STAR program through the National Center for Environmental Research (NCER) under grant R833748 and by the U.S. Department of Energy through the National Energy Technology Laboratory under grant 41817M203841817M2000. This paper has not been subject to EPA's required peer and policy review, and therefore does not necessarily reflect the views of the Agency. No official endorsement should be inferred.

Supporting Information Available

Additional information on the methods used and results described in this paper. This material is available free of charge via the Internet at http://pubs.acs.org.

Literature Cited

(1) de Gouw, J. A.; Middlebrook, A. M.; Warneke, C.; Goldan, P. D.; Kuster, W. C.; Roberts, J. M.; Fehsenfeld, F. C.; Worsnop, D. R.; Canagaratna, M. R.; Pszenny, A. A. P.; Keene, W. C.; Marchewka, M.; Bertman, S. B.; Bates, T. S. Budget of organic carbon in a polluted atmosphere: Results from the New England Air Quality Study in 2002. *J. Geophys. Res.-Atmos.* **2005**, *110* (D16), 16305–16327.

(2) Robinson, A. L.; Donahue, N. M.; Shrivastava, M. K.; Weitkamp, E. A.; Sage, A. M.; Grieshop, A. P.; Lane, T. E.; Pierce, J. R.; Pandis, S. N. Rethinking organic aerosols: Semivolatile emissions and photochemical aging. *Science* **2007**, *315* (5816), 1259–1262.

(3) Grieshop, A. P.; Donahue, N. M.; Robinson, A. L. Laboratory investigation of photochemical oxidation of organic aerosol from wood fires, Part 2: Analysis of aerosol mass spectrometer data. *Atmos. Chem. Phys.* **2009**, *9*, 2227–2240.

(4) Weitkamp, E. A.; Sage, A. M.; Pierce, J. R.; Donahue, N. M.; Robinson, A. L. Organic aerosol formation from photochemical oxidation of diesel exhaust in a smog chamber. *Environ. Sci. Technol.* **2007**, *41* (20), 6969–6975.

(5) Shrivastava, M. K.; Lane, T. E.; Donahue, N. M.; Pandis, S. N.; Robinson, A. L. Effects of gas particle partitioning and aging of primary emissions on urban and regional organic aerosol concentrations. *J. Geophys. Res.* **2008**, *113*, D18301; doi:10.1029/2007JD009735.

(6) Koo, B. Y.; Ansari, A. S.; Pandis, S. N. Integrated approaches to modeling the organic and inorganic atmospheric aerosol components. *Atmos. Environ.* **2003**, *37* (34), 4757–4768.

(7) Schauer, J. J.; Kleeman, M. J.; Cass, G. R.; Simoneit, B. R. T. Measurement of emissions from air pollution sources. 2. C-1 through C-30 organic compounds from medium duty diesel trucks. *Environ. Sci. Technol.* **1999**, *33* (10), 1578–1587.

(8) Kadowaki, S. Characterization of carbonaceous aerosols in the Nagoya urban area. 2. Behavior and origin of particulate n-alkanes. *Environ. Sci. Technol.* **1994**, *28* (1), 129–135.

(9) Pankow, J. F.; Asher, W. E. SIMPOL.1: a simple group contribution method for predicting vapor pressures and enthalpies of vaporization of multifunctional organic compounds. *Atmos. Chem. Phys.* **2008**, *8* (10), 2773–2796.

(10) Lim, Y. B.; Ziemann, P. J. Effects of Molecular Structure on Aerosol Yields from OH Radical-Initiated Reactions of Linear, Branched, and Cyclic Alkanes in the Presence of NO_x. *Environ. Sci. Technol.* **2009**, *43* (7), 2328–2334.

(11) Chan, A. W. H.; Kautzman, K. E.; Chhabra, P. S.; Surratt, J. D.; Chan, M. N.; Crounse, J. D.; Kürten, A.; Wennberg, P. O.; Flagan, R. C.; Seinfeld, J. H. Secondary organic aerosol formation from photooxidation of naphthalene and alkylnaphthalenes: implications for oxidation of intermediate volatility organic compounds (IVOCs). *Atmos. Chem. Phys.* **2009**, *9* (9), 3049–3060.

(12) Presto, A. A.; Miracolo, M. A.; Kroll, J. H.; Worsnop, D. R.; Robinson, A. L.; Donahue, N. M. Intermediate-Volatility Organic Compounds: A Potential Source of Ambient Oxidized Organic Aerosol. *Environ. Sci. Technol.* **2009**, *43* (13), 4744–4749.

(13) Liang, F.; Lu, M.; Keener, T. C.; Liu, Z.; Khang, S. J. The organic composition of diesel particulate matter, diesel fuel and engine oil of a non-road diesel generator. *J. Environ. Monit.* **2005**, *7* (10), 983–988.

(14) Brandenberger, S.; Mohr, M.; Grob, K.; Neukomb, H. P. Contribution of unburned lubricating oil and diesel fuel to particulate emission from passenger cars. *Atmos. Environ.* **2005**, *39* (37), 6985–6994.

(15) Grieshop, A. P.; Miracolo, M. A.; Donahue, N. M.; Robinson, A. L. Constraining the Volatility Distribution and Gas-Particle Partitioning of Combustion Aerosols Using Isothermal Dilution and Thermodenuder Measurements. *Environ. Sci. Technol.* **2009**, *43* (13), 4750–4756.

(16) Ng, N. L.; Chhabra, P. S.; Chan, A. W. H.; Surratt, J. D.; Kroll, J. H.; Kwan, A. J.; McCabe, D. C.; Wennberg, P. O.; Sorooshian, A.; Murphy, S. M.; Dalleska, N. F.; Flagan, R. C.; Seinfeld, J. H. Effect of NO_x level on secondary organic aerosol (SOA) formation from the photooxidation of terpenes. *Atmos. Chem. Phys.* **2007**, *7* (19), 5159–5174.

(17) Atkinson, R.; Arey, J. Atmospheric degradation of volatile organic compounds. *Chem. Rev.* **2003**, *103* (12), 4605–38.

(18) Sage, A. M.; Weitkamp, E. A.; Robinson, A. L.; Donahue, N. M. Evolving mass spectra of the oxidized component of organic aerosol: results from aerosol mass spectrometer analyses of aged diesel emissions. *Atmos. Chem. Phys.* **2008**, *8* (5), 1139–1152.

(19) DeCarlo, P. F.; Dunlea, E. J.; Kimmel, J. R.; Aiken, A. C.; Sueper, D.; Crounse, J.; Wennberg, P. O.; Emmons, L.; Shinozuka, Y.; Clarke, A.; Zhou, J.; Tomlinson, J.; Collins, D. R.; Knapp, D.; Weinheimer, A. J.; Montzka, D. D.; Campos, T.; Jimenez, J. L. Fast airborne aerosol size and chemistry measurements above Mexico City and Central Mexico during the MILAGRO campaign. *Atmos. Chem. Phys.* **2008**, *8* (14), 4027–4048.

(20) Smith, J. D.; Kroll, J. H.; Cappa, C. D.; Che, D. L.; Liu, C. L.; Ahmed, M.; Leone, S. R.; Worsnop, D. R.; Wilson, K. R. The heterogeneous reaction of hydroxyl radicals with sub-micron squalane particles: a model system for understanding the oxidative aging of ambient aerosols. *Atmos. Chem. Phys.* **2009**, *9* (9), 3209–3222.

(21) Seinfeld, J. H., Pandis S. N. *Atmospheric Chemistry and Physics*; John Wiley & Sons, Inc.: New York, 2006.

(22) Hearn, J. D.; Smith, G. D. A mixed-phase relative rates technique for measuring aerosol reaction kinetics. *Geophys. Res. Lett.* **2006**, *33*, DOI:10.1029/2006GL02696.

(23) Williams, B. J.; Goldstein, A. H.; Kreisberg, N. M.; Hering, S. V. An in-situ instrument for speciated organic composition of atmospheric aerosols: Thermal Desorption Aerosol GC/MS-FID (TAG). *Aerosol Sci. Technol.* **2006**, *40* (8), 627–638.

(24) Grieshop, A. P.; Donahue, N. M.; Robinson, A. L. Is the gas-particle partitioning in alpha-pinene secondary organic aerosol reversible? *Geophys. Res. Lett.* **2007**, *34*, L14810; doi: 10.1029/2007GL029987.

(25) Asa-Awuku, A.; Miracolo, M. A.; Kroll, J. H.; Robinson, A. L.; Donahue, N. M. Mixing and phase partitioning of primary and secondary organic aerosols. *Geophys. Res. Lett.* **2009**, *36*, L15827; doi: 10.1029/2009gl039301.

(26) Zhang, Q.; Alfarra, M. R.; Worsnop, D. R.; Allan, J. D.; Coe, H.; Canagaratna, M. R.; Jimenez, J. L. Deconvolution and quantification of hydrocarbon-like and oxygenated organic aerosols based on aerosol mass spectrometry. *Environ. Sci. Technol.* **2005**, *39* (13), 4938–4952.

(27) Donahue, N. M.; Robinson, A. L.; Pandis, S. N. Atmospheric organic particulate matter: From smoke to secondary organic aerosol. *Atmos. Environ.* **2009**, *43* (1), 94–106.

(28) Aiken, A. C.; Decarlo, P. F.; Kroll, J. H.; Worsnop, D. R.; Huffman, J. A.; Docherty, K. S.; Ulbrich, I. M.; Mohr, C.; Kimmel, J. R.; Sueper, D.; Sun, Y.; Zhang, Q.; Trimborn, A.; Northway, M.; Ziemann, P. J.; Canagaratna, M. R.; Onasch, T. B.; Alfarra, M. R.; Prevot, A. S.; Dommen, J.; Duplissy, J.; Metzger, A.; Baltensperger, U.; Jimenez, J. L. O/C and OM/OC ratios of primary, secondary, and ambient organic aerosols with high-resolution time-of-flight aerosol mass spectrometry. *Environ. Sci. Technol.* **2008**, *42* (12), 4478–4485.

(29) Lim, Y. B.; Ziemann, P. J. Products and mechanism of secondary organic aerosol formation from reactions of n-alkanes with OH radicals in the presence of NO_x. *Environ. Sci. Technol.* **2005**, *39* (23), 9229–36.

(30) Capes, G.; Johnson, B.; McFiggans, G.; Williams, P. I.; Haywood, J.; Coe, H. Aging of biomass burning aerosols over West Africa: Aircraft measurements of chemical composition, microphysical properties, and emission ratios. *J. Geophys. Res.* **2008**, *113*, D00C15; doi:10.1029/2008JD009845.

ES902635C